



Feasibility of emulsion-filled pea protein-collagen-carrageenan hydrogel for 3D printing

Ieva Bartkuvienė^{a,*}, Viktorija Eisinaite^a, Evren Gölge^b, Daiva Leskauskaitė^a

^a Department of Food Science and Technology, Kaunas University of Technology, Lithuania

^b Department of Nanotechnology Engineering Sivas Cumhuriyet University, Turkey

1. Introduction

3D printing is a novel approach for shaping foods, allowing precise control over shape, texture, and ingredient distribution, and creating customized food products for individuals with personalized nutrition needs (Pan et al., 2022). Among the various 3D printing techniques, extrusion-based 3D printing is one of the most widely used because of its simplicity and broad compatibility with diverse materials (Zhu et al., 2024). However, the rheological properties of 3D printing ink have specific requirements—the ink must exhibit lower viscosity during ejection from the 3D printer nozzle and regain higher viscosity after extrusion to maintain the shape and provide self-support for the printed structure (Sharma et al., 2024). Therefore, the printability of food is typically assessed through rheological measurements across three sub-phases: extrusion (flow properties), recovery (thixotropic behavior), and regeneration or self-supporting (structural stability), highlighting their critical role in successful printing (Derossi et al., 2024).

The 3D printing of hydrogels can face various difficulties. Incorporating oil into a gel system is a way to improve both extrudability and self-supporting performance due to its lubricating and filling effects on food (Mu et al., 2023). For instance, Zhao et al. (2022) observed that incorporating 20–70 % oil into starch hydrogels enhanced gel strength, attributing this improvement to the filling of gel pores with oil droplets. Several studies (Liu & Ciftci, 2021; Reche et al., 2024) showed that inks with a higher oil content produced shapes that more closely resembled the desired design, thereby enhancing printability. As a result, emulsion-filled gels (EFGs), formed by entrapping dispersed oil droplets within a three-dimensional hydrogel network (Dickinson, 2012), have attracted significant attention as promising candidates for 3D printing inks.

The interactions between oil droplets and the hydrogel matrix have a significant impact on the EFG properties and structure (Foegeding et al., 2017). One of the factors that affects these interactions is the type of emulsifier used. Common emulsifiers in food systems include

low-molecular-weight surfactants (e.g., lecithin, mono- and diglycerides of fatty acids) and biopolymers (Carrera Sánchez & Rodríguez Patino, 2021; Maier et al., 2014). Emulsifiers reduce interfacial tension through adsorption at the oil–water interface, enhancing the kinetic stability of the emulsions (McClements, 2016, p. 3). Low-molecular-weight surfactants adsorb rapidly and strongly to fluid interfaces, resulting in dense molecular packing and low surface and interfacial tensions. In contrast, biopolymer-based emulsifiers (e.g., proteins) attach to the oil droplet at a slower rate and at multiple sites, forming thicker, more structured interfacial layers that enhance droplet–matrix interactions via hydrogen bonding or steric entanglement (Z. Cai et al., 2023; Carrera Sánchez & Rodríguez Patino, 2021). Based on their interaction with the gel matrix, emulsion droplets are classified as either active or inactive fillers. Inactive fillers have low chemical affinity and minimal interaction with the gel matrix, typically reducing gel strength. Conversely, active fillers engage with the gel matrix through noncovalent or covalent interactions, promoting the formation and stabilization of the gel network (Dickinson, 2012; Farjami & Madadlou, 2019).

To date, several attempts have been made to use 3D-print protein-based emulgel systems. Herrera-Lavados et al. (2023) successfully produced 3D printed emulsion gels with low oil content (5 %), containing up to 10 % bean protein and 1–2.5 % gelatin, demonstrating good performance and printability. Similarly, 3D printing ink with good stability and printability was investigated by Yu et al. (2022, 2023), who found that, via the addition of a small amount of polysaccharides (up to 0.5 % of xanthan and guar gums), the 3D printing performance of 6 % soy protein emulsion gel inks could be improved. In addition, a study by Zhu et al. (2024) found that emulgel systems composed of SPI-PP protein (6–12 %) and canola oil (20–80 %) were suitable for 3D printing. EFGs with active fillers were obtained at oil volume fraction (ϕ) up to 0.74, while high internal phase emulsions were obtained at higher values ($>0.74 \phi$). Even though these studies achieved good 3D printing parameters, the protein content in the investigated inks was low, which makes these systems unfavorable for older adults or people during

* Corresponding author.

E-mail address: ieva.jureviciute@ktu.lt (I. Bartkuvienė).

<https://doi.org/10.1016/j.lwt.2025.117749>

Received 20 December 2024; Received in revised form 6 March 2025; Accepted 5 April 2025

Available online 8 April 2025

0023-6438/© 2025 The Authors. Published by Elsevier Ltd. This is an open access article under the CC BY-NC license (<http://creativecommons.org/licenses/by-nc/4.0/>).

periods of active growth, such as pregnancy, lactation, and childhood (Morgan et al., 2023).

Considering that sufficient protein content should be ensured when developing 3D printing inks for personalized nutrition, we attempted to compose high-protein content EFGs suitable for 3D printing applications. In this work, pea proteins were chosen as a source of protein for their significant advantages, including high digestibility, low allergenicity (Y. Wang et al., 2023), and complete amino acid profile, offering high levels of lysine and threonine (Shanthakumar et al., 2022). Due to the well-known functional limitations of pea proteins, such as weak hydrogel formation, a blend of pea proteins with collagen and κ -carrageenan was used in this study to improve the technofunctional characteristics of pea proteins (Kuang et al., 2023). This decision was supported by extensive research dedicated to enhancing the gel strength of pea protein by mixing them with κ -carrageenan (W. Cai et al., 2021; Fu et al., 2023), pectin (D. Zhang, Kobata, et al., 2022; Z. Zhang, Kobata, et al., 2022), modified starch (Y. Wang et al., 2023), chitosan (Xu & Dumont, 2015), gum arabic (Basyigit, 2023), curdlan (Fu et al., 2023), egg white (Kuang et al., 2023), whey (Tarrega et al., 2012; Wong et al., 2013), or myofibrillar fish proteins (Ye et al., 2024). This study aimed to develop high-protein content EFGs with customized rheological and structural properties optimized for 3D printing applications. The objective of this study was to evaluate how oil droplets stabilized with different stabilizers (lecithin or mono- and diglycerides) incorporated into a pea protein–collagen– κ -carrageenan hydrogel affect the printability, mechanical strength, and stability of high-protein content EFGs. The formulated EFGs were thoroughly characterized using rheological and microstructural analyses as well as freezing-thawing, heating-cooling stability tests, and 3D printability assessments.

2. Materials and methods

2.1. Materials

Canola oil was purchased from a local supermarket. Pea protein and collagen (bovine I and III type mixture) isolates containing 80 % and 90 % protein, respectively, were purchased from My Protein (Manchester, UK). κ -Carrageenan was obtained from Sigma-Aldrich (Steinheim, Germany). Soy lecithin was generously provided by the Alvas Group (Kaunas, Lithuania). Mono- and diglycerides of fatty acids (MDGs) were purchased from Puratos (Bijgaarde, Belgium). Potassium chloride and other chemicals were purchased from Eurochemicals (Vilnius, LT). All chemicals were of analytical grade.

2.2. Sample preparation

First, κ -CAR (0.6 % (w/w)), collagen (12.5 % (w/w)), KCl 0.1 % (w/w) and pea protein 12.5 % (w/w) were hydrated together in distilled water for 2 h. The mixture was then heated in a 95 °C water bath for 30 min. To obtain EFGs, the heated mixture was homogenized with different heated oil phases: oil without additives (EFG_Oil), oil containing 1 % soy lecithin (EFG_Oil/Lecithin), and oil containing 2 % mono- and diglycerides of fatty acids (EFG_Oil/MDG). Samples were homogenized at 15,000 rpm (T 18 digital ULTRA-TURRAX, IKA, Germany) at 95 °C for 2 min, with a hydrogel or oil mixing ratio of 80:20. All samples contained a final protein content of 20 % (comprising 10 % pea protein and 10 % collagen) and an oil content of 20 %. After being cooled to room temperature, the gels were stored at 4 °C for 24 h before further analysis.

2.3. Rheological analysis

Rheological properties were characterized using an MCR92 rheometer (Anton Paar, Graz, Austria) with a parallel plate setup (PP25 geometry, 1 mm gap).

The frequency sweep of EFGs was conducted within the linear

viscoelastic region at 25 °C at 1 % strain, while the oscillation frequency ranged from 1 to 100 rad/s. A temperature sweep was conducted on freshly prepared EFG samples, measuring the storage modulus (G') and loss modulus (G'') as the temperature decreased from 95 °C to 25 °C. The samples were then held at 25 °C for 10 min, followed by a second heating-cooling cycle (from 25 °C to 95 °C and back to 25 °C) and another 10-min hold at 25 °C. The strain was set to 1 %, and the heating or cooling rate was 5 °C/min. Silicon oil and solvent traps were used to prevent water evaporation.

The yield stress and thixotropic recovery of EFGs were determined at 30 °C, 35 °C, 40 °C, and 45 °C. Prior to analysis, the samples were heated to approximately 60 °C to ensure they were in a flowable state. Yield stress measurements were carried out in oscillation stress sweep mode at 1 rad/s in the 1 to 1,000 Pa range. According to Z. Liu et al. (2019), the yield stress was determined as a point at which the storage modulus was equal to the loss modulus. Thixotropic recovery was measured using PP50S geometry to prevent the sample from slipping out of the plate-plate system. Samples were subjected to a low shear rate of 1 s⁻¹ for 3 min, followed by a high shear rate of 100 s⁻¹ for 2 min, a 10-min rest period, and a final low shear rate of 1 s⁻¹ for another 3 min. The shear recovery of the EFGs was determined by calculating the percentage of viscosity at the end of the final low shear rate phase relative to the viscosity measured after the initial low shear rate phase.

2.4. SEM

The samples were lyophilized with Alpha 1–4 LSC freeze drier (Martin Christ, Germany) for 18 h at 1 mbar, with the condenser temperature set to −55 °C. Consequently, the oil phase was removed according to the method described by X. Li et al. (2021) by performing oil extraction with petroleum ether, followed by vacuum drying at 50 °C. The Mira3 XMU A Tescan (Tescan Inc., Czech Republic) brand scanning electron microscope (SEM) was used to examine the microstructure of the products. Samples were secured to the SEM Al stubs and then coated with gold 5 nm thick in a Quorum Q150 model Au sputter coating unit (Quorum Tech, GB). The samples were acquired and imaged at a working range of 10 mm using a Tescan Mira3 XMU (Czech Republic) at 10 kV field emission using a back-scattered electron (BSE) detector, and representative images were recorded at different magnifications of 500× and 2,000×.

2.5. Particle size distribution

The particle size distribution of the EFGs was measured using a laser diffraction particle size analyzer Mastersizer 2000 (Malvern, Worcestershire, UK). The refraction indexes for oil and water were 1.47 and 1.33, respectively.

2.6. Heating-cooling and freezing-thawing stability

Five cycles of EFG heating-cooling stability were evaluated. Samples were heated for 30 min in a 95 °C water bath and then cooled at room temperature for 1 h. The procedure was repeated five times, and after each cycle, the visual appearance of the EFGs was evaluated. For freezing-thawing stability, samples were exposed to 5 cycles of freezing at −20 °C for 24 h and thawing at room temperature for 6 h. After each cycle, visual appearance, water-holding capacity (WHC), and oil-holding capacity (OHC) were evaluated.

2.7. Water- and oil-holding capacity

The WHC and OHC of the EFGs were assessed by adding 5 g of the sample to 15 mL centrifuge tubes and centrifuging at 10,000×g for 20 min at room temperature (Digitor 21R, Orto Alresa, Greece). The oil and water released from the samples were carefully collected with a syringe and weighed. WHC and OHC were calculated using the following

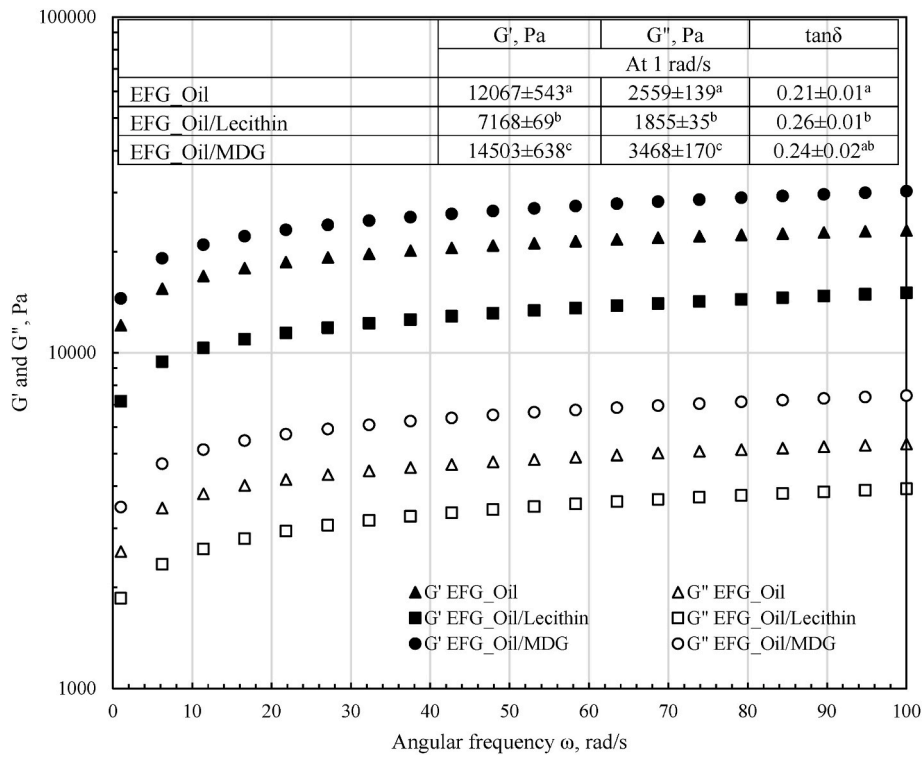


Fig. 1. Frequency sweep of emulsion-filled gels. Table depicts storage modulus, loss modulus and $\tan\delta$ of EFG at 1 rad/s.

formula:

$$\text{Solvent holding capacity (\%)} = \left(1 - \frac{w_1}{w_2}\right) \times 100 \quad (1)$$

where w_1 is the oil (or water) content (g) released from the sample after centrifugation, and w_2 is the oil (or water) content (g) in the sample.

2.8. 3D printing

An extrusion-based 3D printer (FOODINI, Natural Machines, Spain) was used to evaluate the printability of the EFGs. The printing parameters selected during pre-testing included a nozzle diameter of 4 mm, printing speed of 8,000 mm min⁻¹, and line thickness of 4.2 mm. Before the 3D printing procedure, the EFGs were heated to approximately 60 °C to achieve a flowable state and then transferred to preheated 100 mL capsules (at 30 °C, 35 °C, 40 °C, or 45 °C). They were maintained at these temperatures for 30 min to ensure uniform temperature distribution. The selected shape for the 3D printing experiment was a 15-layer hollow cylinder (30 mm diameter, 4.2 mm wall width, and 63 mm height). 3D printing accuracy and stability were calculated according to the modified (Y. Liu et al., 2022) formulas:

$$3D \text{ printing accuracy (\%)} = \frac{\left(1 - \frac{h_0 - h}{h}\right) + \left(1 - \frac{d_0 - d}{d}\right) + \left(1 - \frac{w_0 - w}{w}\right)}{3} \times 100 \quad (2)$$

$$3D \text{ printing stability (\%)} = \frac{\left(1 - \frac{h_2 - h_0}{h_0}\right) + \left(1 - \frac{d_2 - d_0}{d_0}\right) + \left(1 - \frac{w_2 - w_0}{w_0}\right)}{3} \times 100 \quad (3)$$

where h_0 is the average height, d_0 is the average diameter, and w_0 is the average wall width of the 3D-printed cylinder immediately after printing; h_2 , d_2 , and w_2 are the height, diameter, and wall width of the 3D-

printed cylinder 2 h after printing; and h , d , and w are the height, diameter, and wall width of the designed model, respectively.

2.9. Statistical analysis

All experiments were carried out at least three times, and the results were expressed as the mean ± standard deviation. A *t*-test was employed to identify significant differences between samples, with a *p*-value below 0.05 considered statistically significant. Data analysis was performed using Graph Pad Prism software.

3. Results and discussion

3.1. Rheological and microstructural characterization of EFGs obtained by the addition of oil with or without different stabilizers

The suitability of EFGs for 3D printing applications was assessed through rheological evaluation. Extrusion and recovery properties were evaluated by measuring yield stress and thixotropic behavior, while self-supporting properties were measured by frequency and temperature sweeps.

3.1.1. Frequency sweep

The oscillation frequency sweep measurement results of the different EFGs are presented in Fig. 1. All systems exhibited gel behavior when G' was higher than G'' in the entire frequency range from 1 to 100 rad/s within their LVR, and the loss factor $\tan\delta$ was <1 (D'Alessio et al., 2024). According to the frequency dependence of the moduli, the structural stability of the EFGs can be judged (Kurt & Genççelep, 2018). A moderate increase in G' and G'' with increasing frequency was registered because the structural elements of the EFGs did not have enough time to rearrange themselves upon stress applied at the high-frequency range, resulting in stiffer structures (Lin et al., 2024). Additionally, the values of G' and G'' for the different EFGs were different. Higher G' and G'' values were determined for the EFG_Oil/MDG and EFG_Oil, indicating that they were more solid-like in comparison with the EFG_Oil/Lecithin.

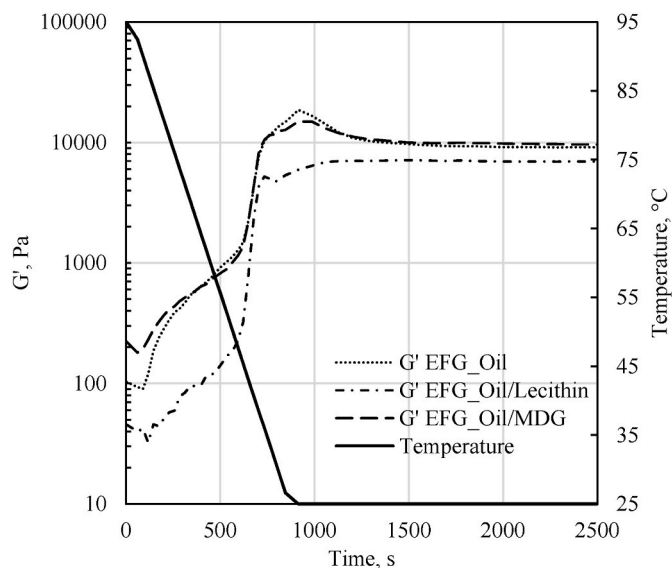


Fig. 2. Temperature sweep of emulsion-filled gels.

The observed differences might have contributed to the size and distribution of the embedded oil droplets in the structure of the EFG. The wider distribution of larger oil droplets observed in the EFG_Oil/Lecithin might trigger its lower hardness (Fig. 5) (Luo et al., 2019). Mechanical strength is an important characteristic of the EFG's printability since materials with weak structural stability deform more easily during extrusion, causing low smoothness of the extruded filaments (Mu et al., 2023). A higher G' value indicates stronger mechanical strength of the EFG and its capability to support its weight after printing (Y. Liu et al., 2018).

3.1.2. Temperature sweep

Temperature sweeps were used to investigate structural changes that can occur during sol–gel transition processes, which are most important for solidifying EFGs after extrusion. The results are demonstrated in Fig. 2. As shown in our previous studies during the cooling process, the pea protein-collagen-carrageenan-based macromolecular structure gradually transits from highly flexible and single random coils of collagen and carrageenan molecules mixed with the pea protein aggregates toward a physically interacted interpenetrating gel network

consisting of mono or triple helices and aggregated structures with reduced mobility of molecules (Bartkuvienė et al., 2024). Accordingly, a sharp increase in G' values of all investigated EFGs during the temperature decrease period from 95 °C to 25 °C was recorded, implying the onset of gelation. Systems with rapid thermosetting gelation properties are highly valuable as 3D printing inks (Y. Liu et al., 2024). In our case, the sharpest G' increase was recorded during the temperature decrease from 45 °C to 30 °C for all samples. However, the lowest G' values in this temperature interval were determined for the EFG_Oil/Lecithin; the G' increased from 0.32 kPa to 4.97 kPa. The G' of the EFG_Oil changed from 1.49 to 13.91 kPa, and the G' of the EFG_Oil/MDG raised from 1.37 kPa to 12.474 kPa, as the temperature decreased from 45 °C to 30 °C. During the incubation period, when the temperature was maintained at 25 °C, the G' values remained almost unchanged for 25 min. This indicates that the EFG structure has reached equilibrium, supporting the deposited layers and maintaining the desired shape during 3D printing (Chen et al., 2019). Considering the influence of different stabilizers used in the oil added as a gel filler, they did not affect the shape of the recorded temperature sweep curves. However, adding lecithin-stabilized oil resulted in lower EFG G' values over the entire temperature range.

3.1.3. Yield stress

The yielding behavior of matrices can be an advantage in 3D printing, as it allows the formation of specific, original shapes during the flow stage, which the fluid will essentially keep (Geffrault et al., 2023). Fig. 3 presents the yield stress as the minimum force required to start the flow of EFGs, which were obtained by adding oil with different stabilizers and measured at different temperatures. Relatively low yield stress values under shear are reported as desired during extrusion in 3D printing (Mu et al., 2023). The lowest yield stress was determined for the EFG_Oil/Lecithin; it was 2,569–2,965 Pa. When oil stabilized with MDG was added to the gel, a slightly higher yield stress was recorded (3,057–3,451 Pa). However, the yield stress increased the most when oil without stabilizers was used in the EFG. These results confirm the frequency sweep results, which also showed the contribution of the oil stabilizer used to the mechanical strength of the EFG.

The observed differences in the rheological properties of EFGs might be due to factors such as oil/filler and hydrogel/matrix characteristics and interactions between them (Farjami & Madadlou, 2019). First, our previous study (Bartkuvienė et al., 2024) showed the presence of non-network pea proteins in the pea protein-carrageenan hydrogel, which can act as emulsifiers by adsorbing on the O/W interface of oil droplets (Olsmats & Rennie, 2024). Second, the competitive or

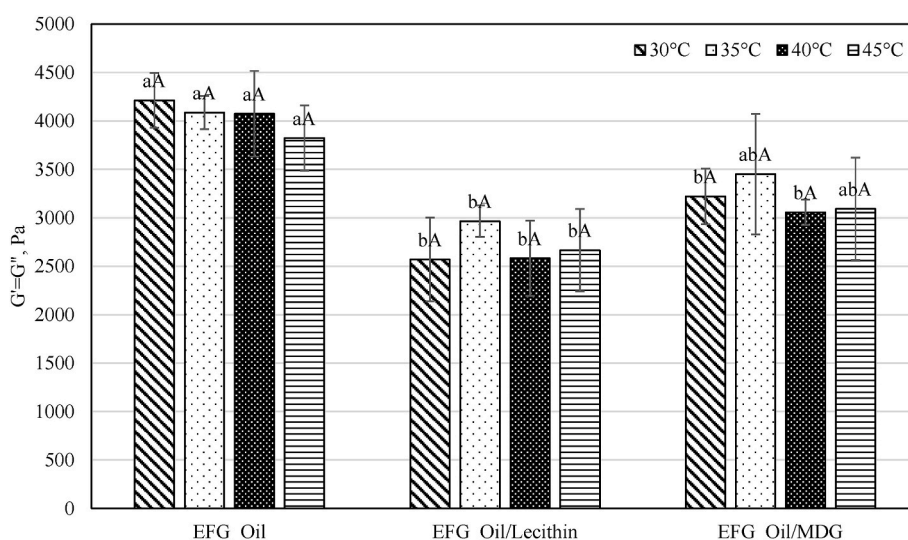


Fig. 3. The yield stress of emulsion-filled gels measured at different temperatures (30 °C, 35 °C, 40 °C and 45 °C). Different letters among columns indicate significant ($P < 0.05$) differences: lowercase – among different EFGs at similar temperatures; uppercase – among different temperatures of EFGs.

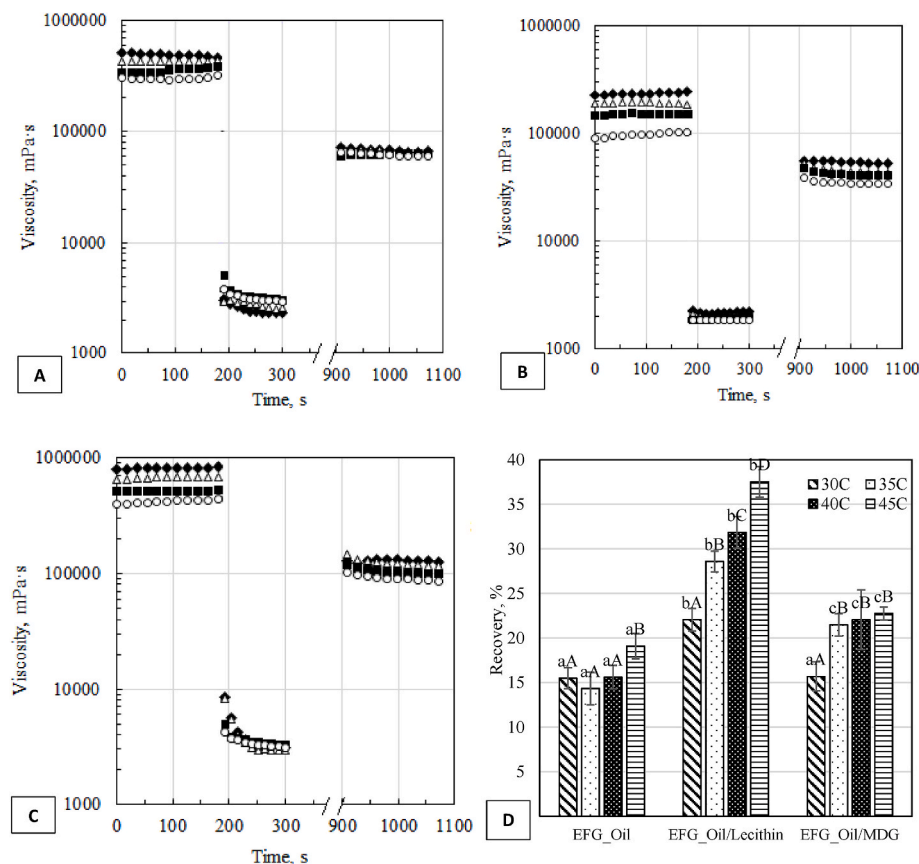


Fig. 4. Thixotropic recovery of emulsion-filled conducted at different temperatures (30 °C (◆), 35 °C (Δ), 40 °C (■) and 45 °C (○)). A – C shows changes in viscosity during low (1/s)–high (100/s)–low (1/s) shear rates of EFG_Oil, EFG_Oil/Lecithin and EFG_Oil/MDG, respectively. D shows the percentage of the shear recovery. Different letters among columns indicate significant ($P < 0.05$) differences: lowercase – among different EFGs at similar temperatures; uppercase – among different temperatures of EFGs.

synergistic adsorption of two types of emulsifiers might occur at the oil droplet interface in the presence of lecithin or MDG. We presume that in the EFG_Oil/Lecithin, oil droplets with lecithin coexist with pea proteins at the interface. The concentration of lecithin is high enough to cover the surface of oil droplets, and its small molecules adsorb faster at the interface than rigid and large protein molecules. As a result, a large amount of unabsorbed protein remains in the dispersed phase (Xia et al., 2024). Therefore, oil droplets act as inactive fillers in the EFG_Oil/Lecithin, with limited interaction with the gel matrix, typically weakening the gel structure (Farjami & Madadlou, 2019). In the case of the EFG_Oil, proteins acted as the sole emulsifier and gelling agent. Oil behaves as an active filler due to the formation of a thick protein layer on the surface of oil droplets interacting with the networking proteins in the gel matrix and strengthening the gel structure (Z. Cai et al., 2023). Finally, oil droplets also act as active fillers in the EFG_Oil/MDG due to the possible interaction between proteins and MDGs at the interface (Loi et al., 2019). For instance, after the absorption of low molecular weight MDGs at the interface of oil droplets, they interacted with proteins in the gel matrix, increasing the gel strength, which made the EFG_Oil flow more difficult under shearing forces. The observed impact of different stabilizers added to the embedded oil droplets on their behavior, as active or inactive fillers in the EFGs, still requires further research to explain the underlying mechanism. Additionally, Fig. 3 clearly shows that temperature had no significant effect on the yield stress value of the EFGs. Temperature sweep curves (Fig. 2) exhibited a drastic increase in G' values during the decrease in temperature, indicating cold-set gel formation by the pea protein-collagen-carrageenan matrix in this range of temperatures. However, the behavior of the oil droplets added as active or inactive fillers in this matrix was more important for the flow

properties of the EFGs under shear. It can be argued that the combined action of the pea protein-collagen-carrageenan network and the emulsion droplet behavior in this network resulted from the yield stress of the EFGs.

3.1.4. Thixotropic recovery

Next, the thixotropic recovery of the EFGs was studied, which shows the ability of matrices to recover their structural organization and viscous properties after shearing and, therefore, plays a critical role in the accuracy and precision of 3D printing (H. Wang et al., 2022). Since the most pronounced increase in G' was recorded in the temperature range from 45 °C to 30 °C, the thixotropic recovery of EFGs was determined at these temperatures.

As seen in Fig. 4A–C, the EFGs' viscosity increased gradually with the temperature decrease in the first low shear stage (1–180 s). Lowering the temperature favored intermolecular interactions between pea proteins, collagen, and carrageenan, reinforcing the interpenetrating network structure strength. This result was observed for all three EFG formulations. During the following high shear stage (180–300 s), the viscosity of all the samples decreased drastically due to the break of the ordered structure of the EFGs. The conditions of this phase of the experiment simulated the moment when the EFG passed through the narrow nozzles of the printer (Z. Liu et al., 2019). In the final recovery stage (900–1080 s), when the shear rate was set back to low, the viscosity quickly recovered in all investigated EFGs but to a different extent. Since the viscosity of the EFGs in the third stage was significantly lower than in the first stage, irreversible structural damage in the emulsion gel can be concluded. However, all EFGs demonstrated a higher and insignificantly different viscosity recovery ability at higher temperatures. Additionally,

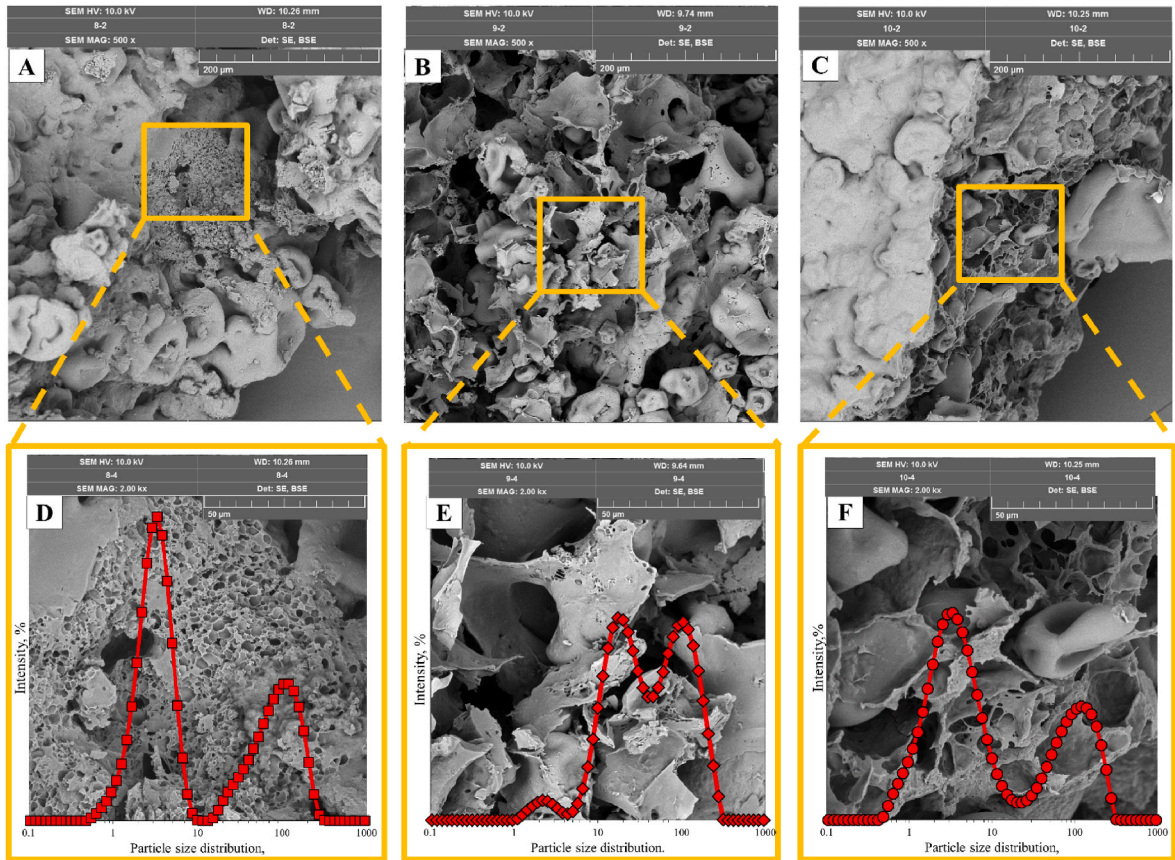


Fig. 5. SEM micrographs and particle size distribution (D–F) of EFGs: EFG_Oil (A, D), EFG_Oil/Lecithin (B, E), and EFG_Oil/MDG (C, F). The top row displays SEM images at 500× magnification, while the bottom row presents images at 2000× magnification.

the EFG_Oil/Lecithin showed the best recoverability of 37.5 % measured at 45 °C. The recovery of EFG_Oil and EFG_Oil/MDG at the same temperature was 19.1 % and 22.7 %, respectively (Fig. 4D). Consequently, the good printability of the EFG_Oil/Lecithin might be predicted due to the highest degree of recovery. Its structure was able to return to a relatively stable state after degradation during extrusion. However, these gels still had the lowest viscosity in the experiment’s first and final

low-shear stages, which could have led to the collapse of their 3D-printed structures (Qiu et al., 2023).

3.1.5. Microstructure analysis

Finally, we analyzed the EFGs’ microstructure to confirm our hypotheses about the differences in the structures obtained by adding oil with different stabilizers. The SEM micrographs captured at 500x and

Table 1
The visual appearance of emulsion-filled gels after each of the five freezing-thawing cycles.



























	Freezing-thawing cycle				
	1	2	3	4	5
EFG_Oil					
EFG_Oil/Lecithin					
EFG_Oil/MDG					

Table 2

3D-printability of emulsion-filled gels at different printing temperatures (30 °C, 35 °C, 40 °C and 45 °C).

		3D-printing temperature			
		30 °C	35 °C	40 °C	45 °C
EFG_Oil	View after printing				
	Printing accuracy, %	–	85.42 ± 1.71	90.43 ± 1.99	–
	Printing stability, %	–	91.52 ± 2.10	95.04 ± 2.00	–
EFG_Oil/Lecithin	View after printing				
	Printing accuracy, %	–	–	–	–
	Printing stability, %	–	–	–	–
EFG_Oil/MDG	View after printing				
	Printing accuracy, %	–	85.02 ± 1.79	86.45 ± 1.82	–
	Printing stability, %	–	96.79 ± 2.04	97.28 ± 2.04	–

2,000× magnifications are shown in Fig. 5. At a lower magnification (Fig. 5A–C), pea protein aggregates of varying sizes formed a connective network together with collagen and κ-CAR. A highly porous structure was observed at a higher magnification (Fig. 5D–F). The circular-shaped pores were believed to have contained oil droplets before they were extracted for SEM analysis. Adding different additives, such as lecithin or MDG, to the oil phase resulted in EFGs with varying pore sizes. In the EFG_Oil sample, where oil without additives acted as an active filler, the pores were predominantly small and uniform (<5 μm), with occasional larger pores observed. In contrast, the pore size distribution in the EFG_Oil/MDG sample was more heterogeneous, ranging from less than 5 μm to approximately 30 μm. In addition, the micrograph of the EFG_Oil/Lecithin revealed significantly larger pore sizes, likely due to the filler particles acting as inactive fillers. Without strong interactions with the gel matrix, these particles tend to coalesce, forming larger oil droplets (R. Li et al., 2023).

Further structural differences among the EFGs were evaluated by measuring their particle size distribution, as shown in Fig. 5(D–F). All EFG samples exhibited multimodal distributions. The EFG_Oil showed two distinct particle size peaks, with maximums of around 3 μm and 120 μm. The particle size distribution curve and SEM micrographs revealed that the first peak corresponded to the oil droplets within the gel. In contrast, the second group represents pea protein aggregates, which also act as fillers within the gel network. The EFG_Oil/MDG sample exhibited similar peaks, although the oil droplet intensity peak was broader, indicating a less homogeneous distribution than that of the EFG_Oil sample. In contrast, the EFG_Oil/Lecithin sample exhibited a different

oil droplet distribution, dominated by larger particle sizes, with two main peaks at 17 μm and 105 μm and a smaller peak at 2 μm. The size and distribution of oil droplets play a crucial role in determining the stability and strength of gels. Narrow size distribution and a smaller mean oil droplet diameter typically result in better mechanical strength and gel stability (Jost, 1993). Due to the dominance of larger oil droplets of varying sizes in the EFG_Oil/Lecithin sample, the gel strength was expected to be significantly lower than in the EFG_Oil and EFG_Oil/MDG samples. This is consistent with the frequency sweep results in Fig. 1, where the EFG_Oil/Lecithin exhibited the lowest G' and G'' values.

3.2. Printability of EFGs

Next, the performance of EFGs in the 3D printing of 15-layer cylinders was studied. As expected, after rheological and microstructural characterization of the different EFG formulations, notable differences in their 3D printability were observed (Table 2). Printing temperature also proved to be important. The EFG_Oil/Lecithin failed to print at all temperatures used in this experiment. Both the EFG_Oil and EFG_Oil/MDG showed better 3D printing behavior with clear structures at 35 °C and 40 °C. The 3D-printed EFG_Oil/MDG exhibited the best printing accuracy (95.04 %) and printing stability (97.28 %) at 40 °C. The exact formulation 3D-printed at 35 °C revealed slightly decreased printing accuracy (85.02 %) and printing stability (96.79 %). Similar trends were observed for the 3D-printed EFG_Oil when printing accuracy and printing stability at 40 °C were 90.43 % and 95.04 %, respectively. However, at 30 °C, printed constructs collapsed upon printing, and 45 °C

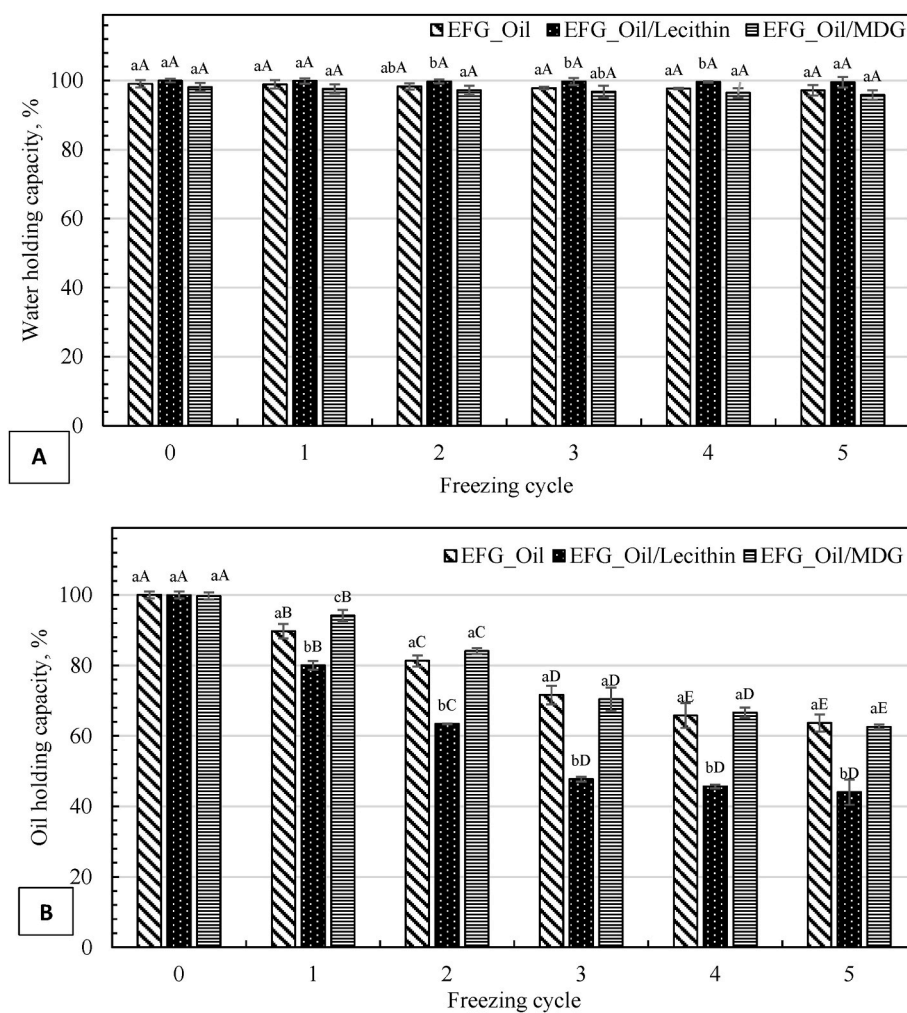


Fig. 6. Water-holding capacity (A) and oil-holding capacity (B) during five freezing-thawing cycles. Different letters among columns indicate significant ($P < 0.05$) differences: lowercase – among different EFGs after each freezing-thawing cycle; uppercase – among different freezing-thawing cycles of EFGs.

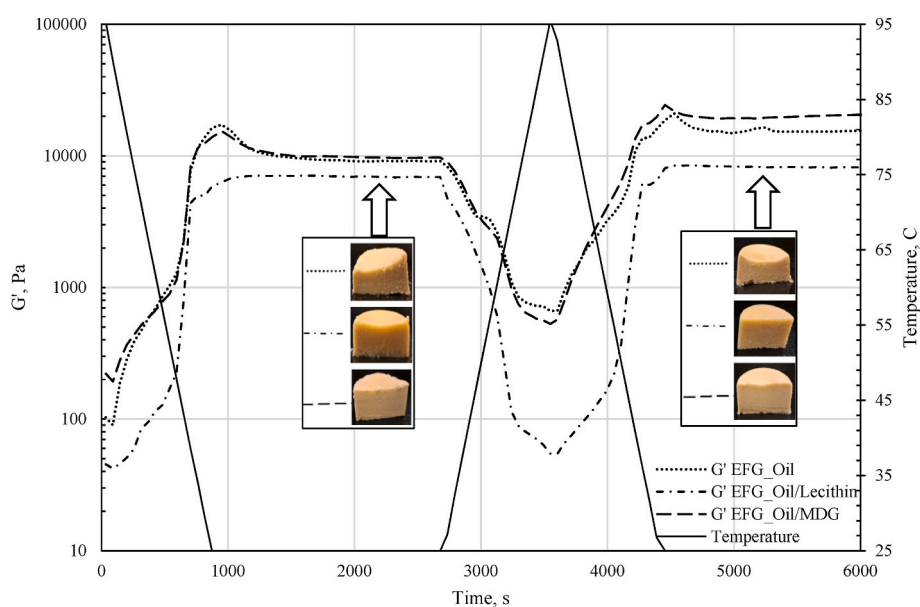


Fig. 7. Temperature dependence of storage modulus during heating and cooling cycles. Photos indicate the visual appearance of emulsion-filled gels at the end of each heating-cooling cycle.

was not a suitable temperature for printing these EFGs.

Extrudability and self-supporting capacity are two main characteristics of 3D printing formulations (Cheng et al., 2024). In this study, EFG extrudability was evaluated as yield stress and thixotropic recovery, and the self-supporting capacity was related to the mechanical strength of the gels. Among the EFGs, the EFG_Oil/Lecithin showed the best recoverability and the lowest yield point, suggesting the best extrudability of these formulations. However, the low viscosity and mechanical strength of the EFG_Oil/Lecithin hindered the ability of the lower layers to support the upper layers during printing (Z. Liu et al., 2019). The EFG_Oil and EFG_Oil/MDG demonstrated good printing behavior attributed to the increased storage modulus G' (Fig. 1) and higher viscosity after extrusion (Fig. 4), which ensured the structural integrity of these EFGs post-printing (Joshi et al., 2024). In summary, the results of the EFGs' printability further corroborated the involvement of stabilizers added into the oil phase in the formation of high-protein EFGs. The oil functioning as an active filler in the EFGs might significantly improve their 3D printing performance.

3.3. Thermoreversibility and freezing-thawing stability

It is important to determine how 3D-printed EFGs respond to thermal and freezing-thawing processing to evaluate the possibilities of applying them to various technologies. EFG stability under five cycles of freezing-thawing (F-T) treatment was estimated by measuring the WHC and OHC after each cycle of F-T treatment. WHC indicates the interaction between biopolymers and water in the hydrogel network (M. Zhang et al., 2024), and OHC is used as an indicator of the interaction between oil droplets and the hydrogel network (Kang et al., 2024). The results are presented in Fig. 6 and Table 1. All investigated EFGs exhibited self-supporting structures, and differences in oil droplet stabilization did not affect the macromorphology of the EFGs. After the first F-T cycle, the appearance, WHC, and OHC of all EFGs did not change, indicating good stability of the gels. However, significant oil separation occurred in the EFGs after the second F-T cycle. There was a notable difference between the EFGs, demonstrating the lowest OHC for the EFG_Oil/Lecithin (80 %) and higher OHC for the EFG_Oil and EFG_Oil/MDG (89.7 % and 94.1 %, respectively). Further F-T cycles caused a consistent decline in the OHC of the EFGs, most notably in the EFG_Oil/Lecithin. This indicates that the response of gels to freezing and thawing depends on the oil droplet behavior in the EFG structures, whether they are active or inactive fillers. In the EFG_Oil/Lecithin, the oil droplets behaved as inactive fillers with no interactions with hydrogel; therefore, the increase in F-T cycles led to the more extensive accumulation of oil droplets with subsequent separation. Meanwhile, stronger incorporation of oil droplets into the hydrogel in the EFG_Oil and EFG_Oil/MDG better protected them from separation. Interestingly, the F-T treatment had no significant effect on the WHC of all investigated EFGs, demonstrating that the internal bonding between hydrogel components and water was not destroyed during the five F-T cycles.

After being heated at 95 °C, all EFGs maintained their self-supporting structures (Fig. 7). No oil or water was separated from the gels. As shown in Fig. 7, all EFGs demonstrated defined thermoreversibility. Two cooling and heating cycles were performed, and the change in the elastic modulus G' was recorded. During the first cooling cycle from 95 °C to 25 °C, EFG experienced a sharp increase in G' , indicating the interpenetrating hydrogel formation by the pea protein-collagen-carrageenan mixture. All three components of the mixture participated in the cold-set gel formation. Previous studies have demonstrated that hydrogen bonds and hydrophobic interactions are major contributors to gel formation (Bartkuviene et al., 2024). There were no changes in the G' value during the first holding cycle at 25 °C, showing that the gel network was mainly formed during the cooling. Afterward, when the temperature was elevated from 25 °C to 95 °C, a rapid decrease in G' was detected, exhibiting that the hydrogen and hydrophobic interactions had been disrupted and that the gel had been converted back to a liquid

state. During this heating process, hydrogen bonds are essential since hydrogen bonding is exothermic and formed at low temperatures but disrupted at high temperatures (Lu et al., 2022). However, considerably higher G' values were recorded at 95 °C than at the same temperature during the first cycle. This was probably due to the disulfide bonds contributing to the formation of the pea protein network and making them irreversible (S. Zhang et al., 2025). The G' of all EFGs increased during the second cooling cycle, indicating the formation of solid gel, and was consistent during the second holding cycle. Again, higher G' values were determined during the second cooling cycle than during the first cooling cycle. Similar G' changes were observed in thermally reversible pea protein gels studied by (Zhu et al., 2022). They explained this phenomenon by losing water during the reheating process, which increased the protein concentration. Adding different stabilizers to the oil droplets incorporated into the hydrogel network did not affect the structure's thermoreversibility of the hydrogel made from a pea protein-collagen-carrageenan mixture.

4. Conclusions

This study developed three high-protein (20 wt%) EFGs formulated from a pea protein-collagen-carrageenan hydrogel and oil droplets stabilized by different emulsifiers: lecithin (EFG_Oil/Lecithin), mono- and diglycerides of fatty acids (EFG_Oil/MDG), and non-network proteins that were present in the hydrogel (EFG_Oil). The use of different emulsifiers resulted in EFGs with different rheological, structural, and 3D printability characteristics. The differences were explained by oil droplets acting as active or inactive fillers, depending on the emulsifier used. Specifically, the EFG_Oil and EFG_Oil/MDG exhibited superior mechanical strength and 3D printability due to their active filler behavior, where oil droplets strongly interacted with the hydrogel matrix. In contrast, in the EFG_Oil/Lecithin, oil droplets acted as inactive fillers, as the lecithin-coated oil droplets weakened the gel structure. As a result, while the EFG_Oil/Lecithin demonstrated enhanced extrudability, its poor self-supporting capacity led to the collapse of the 3D printed structures.

All three EFGs exhibited good thermoreversibility during heating-cooling cycles, indicating their ability to transition between gel and sol states without phase separation. This property is crucial for 3D printing, as it ensures a consistent flow of heated EFG through the printer nozzle and rapid gelation upon cooling, enabling the creation of well-defined, self-supporting structures. In addition, all three EFGs remained stable during the first freezing-thawing cycle, demonstrating their potential to maintain structural integrity during storage.

These findings demonstrate that high-protein, stable, and thermoreversible EFGs suitable for 3D printing can be achieved by using different emulsifiers to modulate key gel properties—such as extrudability and self-supporting capacity—which are crucial for successful 3D printing.

CRediT authorship contribution statement

Ieva Bartkuviene: Writing – original draft, Methodology, Investigation. **Viktorija Eisinaite:** Methodology, Formal analysis. **Evren Gölge:** Methodology, Investigation. **Daiva Leskauskaitė:** Writing – review & editing, Supervision, Funding acquisition, Data curation, Conceptualization.

Declaration of competing interest

The authors declare that they have no known competing financial interests or personal relationships that could have appeared to influence the work reported in this paper.

Acknowledgment

This project has received funding from the Research Council of Lithuania (LMTLT), agreement no. S-A-UEI-23-1 (22-12-2023).

Data availability

Data will be made available on request.

References

- Bartkuvienė, I., Kersienė, M., Petrikaitė, V., & Leskauskaitė, D. (2024). Modulation of pea protein isolate hydrogels by adding kappa-carrageenan: Gelling properties and formation mechanism. *International Journal of Food Science and Technology*, 59(9), 6598–6610. <https://doi.org/10.1111/ijfs.17413>
- Basyigit, B. (2023). Designing nanoliposome-in-natural hydrogel hybrid system for controllable release of essential oil in gastrointestinal tract: A novel vehicle. *Foods*, 12(11), 2242. <https://doi.org/10.3390/foods12112242>
- Cai, W., Huang, W., & Chen, L. (2021). Soluble pea protein aggregates form strong gels in the presence of κ-carrageenan. *ACS Food Science & Technology*, 1(9), 1605–1614.
- Cai, Z., Wei, Y., Shi, A., Zhong, J., Rao, P., Wang, Q., & Zhang, H. (2023). Correlation between interfacial layer properties and physical stability of food emulsions: Current trends, challenges, strategies, and further perspectives. *Advances in Colloid and Interface Science*, 313, Article 102863. <https://doi.org/10.1016/j.cis.2023.102863>
- Carrera Sánchez, C., & Rodríguez Patino, J. M. (2021). Contribution of the engineering of tailored interfaces to the formulation of novel food colloids. *Food Hydrocolloids*, 119, Article 106838. <https://doi.org/10.1016/j.foodhyd.2021.106838>
- Chen, J., Mu, T., Goffin, D., Blecker, C., Richard, G., Richel, A., & Haubruge, E. (2019). Application of soy protein isolate and hydrocolloids based mixtures as promising food material in 3D food printing. *Journal of Food Engineering*, 261, 76–86. <https://doi.org/10.1016/j.jfoodeng.2019.03.016>
- Cheng, Y., Wang, B., Lv, W., Zhong, Y., & Li, G. (2024). Effect of xanthan gum on physicochemical properties and 3D printability of emulsion-filled starch gels. *Food Hydrocolloids*, 149, Article 109613. <https://doi.org/10.1016/j.foodhyd.2023.109613>
- D'Alessio, G., Iervese, F., Valbonetti, L., Faieta, M., Pittia, P., & Di Mattia, C. D. (2024). Tailoring pea proteins gelling properties by high-pressure homogenization for the formulation of a model spreadable plant-based product. *LWT*, 207, Article 116627. <https://doi.org/10.1016/j.lwt.2024.116627>
- Derossi, A., Spence, C., Corradini, M. G., Jekle, M., Fahmy, A. R., Caporizzi, R., Devahastin, S., Moses, J. A., Le-Bail, A., Zhou, W., Zhang, M., Bhandari, B., & Severini, C. (2024). Personalized, digitally designed 3D printed food towards the reshaping of food manufacturing and consumption. *Npj Science of Food*, 8(1), 54. <https://doi.org/10.1038/s41538-024-00296-5>
- Dickinson, E. (2012). Emulsion gels: The structuring of soft solids with protein-stabilized oil droplets. *Food Hydrocolloids*, 28(1), 224–241. <https://doi.org/10.1016/j.foodhyd.2011.12.017>
- Farjami, T., & Madadlou, A. (2019). An overview on preparation of emulsion-filled gels and emulsion particulate gels. *Trends in Food Science & Technology*, 86, 85–94. <https://doi.org/10.1016/j.tifs.2019.02.043>
- Foegeding, E. A., Stieger, M., & Van De Velde, F. (2017). Moving from molecules, to structure, to texture perception. *Food Hydrocolloids*, 68, 31–42. <https://doi.org/10.1016/j.foodhyd.2016.11.009>
- Fu, J., Zheng, Y., Gao, Y., Zhang, Y., Sun, C., & Fang, Y. (2023). Effect of different polysaccharides on the texture and fibrous structure of high-moisture extruded pea protein isolate. *Food Biophysics*, 18(4), 606–618. <https://doi.org/10.1007/s11483-023-09805-7>
- Geffrault, A., Bessaies-Bey, H., Roussel, N., & Coussot, P. (2023). Printing by yield stress fluid shaping. *Additive Manufacturing*, 75, Article 103752. <https://doi.org/10.1016/j.addma.2023.103752>
- Herrera-Lavados, C., Tabilo-Munizaga, G., Rivera-Tobar, D., Carvajal-Mena, N., Palma-Acevedo, A., Moreno-Osorio, L., & Pérez-Won, M. (2023). Development of bean-based emulgels for 3D printing applications: Feasibility for dysphagia diets. *Journal of Food Engineering*, 358, Article 111687. <https://doi.org/10.1016/j.jfoodeng.2023.111687>
- Joshi, S., Sahu, J. K., Prakash, S., & Naik, S. N. (2024). Modulating the 3D printability of vitamin D3-nanoemulsion-based dairy gels: Influence of emulsifier on gel structure, printing behaviour and vitamin D3 retention. *Journal of Food Engineering*, 373, Article 112032. <https://doi.org/10.1016/j.jfoodeng.2024.112032>
- Jost, R. (1993). Functional characteristics of dairy proteins. *Trends in Food Science & Technology*, 4(9), 283–288. [https://doi.org/10.1016/0924-2244\(93\)90071-H](https://doi.org/10.1016/0924-2244(93)90071-H)
- Kang, Y., Ng, S. M., Aruchunan, U., Ma, X., & Sim, S. Y. J. (2024). Development of non-animal chicken fat using faba bean protein-based emulsion gels. *LWT*, 214, Article 117124. <https://doi.org/10.1016/j.lwt.2024.117124>
- Kuang, J., Hamon, P., Lechevalier, V., & Saurel, R. (2023). Thermal behavior of pea and egg white protein mixtures. *Foods*, 12(13), 2528. <https://doi.org/10.3390/foods12132528>
- Kurt, A., & Gençlepe, H. (2018). Enrichment of meat emulsion with mushroom (*Agaricus bisporus*) powder: Impact on rheological and structural characteristics. *Journal of Food Engineering*, 237, 128–136. <https://doi.org/10.1016/j.jfoodeng.2018.05.028>
- Li, X., Guo, C., Li, P., Sun, J., Yang, X., & Guo, Y. (2021). Structural characteristics of gluconic acid δ-lactone induced casein gels as regulated by gellan gum incorporation. *Food Hydrocolloids*, 120, Article 106897. <https://doi.org/10.1016/j.foodhyd.2021.106897>
- Li, R., Wu, N., Xue, H., Gao, B., Liu, H., Han, T., Hu, X., Tu, Y., & Zhao, Y. (2023). Influence and effect mechanism of filler type on the physicochemical properties, microbial numbers, and digestibility of ovalbumin emulsion gels during storage. *Food & Function*, 14(8), 3779–3792. <https://doi.org/10.1039/D2FO03526J>
- Lin, Q., Li, X., McClements, D. J., Jin, Z., Qiu, C., & Li, G. (2024). Plant-based delivery systems for controlled release of hydrophilic and hydrophobic active ingredients: Pea protein-alginate bigel beads. *Food Hydrocolloids*, 154, Article 110101. <https://doi.org/10.1016/j.foodhyd.2024.110101>
- Liu, Z., Bhandari, B., Prakash, S., Mantihal, S., & Zhang, M. (2019). Linking rheology and printability of a multicomponent gel system of carrageenan-xanthan-starch in extrusion based additive manufacturing. *Food Hydrocolloids*, 87, 413–424. <https://doi.org/10.1016/j.foodhyd.2018.08.026>
- Liu, L., & Ciftci, O. N. (2021). Effects of high oil compositions and printing parameters on food paste properties and printability in a 3D printing food processing model. *Journal of Food Engineering*, 288, Article 110135. <https://doi.org/10.1016/j.jfoodeng.2020.110135>
- Liu, Y., Liu, D., Wei, G., Ma, Y., Bhandari, B., & Zhou, P. (2018). 3D printed milk protein food simulant: Improving the printing performance of milk protein concentration by incorporating whey protein isolate. *Innovative Food Science & Emerging Technologies*, 49, 116–126. <https://doi.org/10.1016/j.ifset.2018.07.018>
- Liu, Y., Sun, Q., Wei, S., Xia, Q., Pan, Y., Liu, S., Ji, H., Deng, C., & Hao, J. (2022). LF-NMR as a tool for predicting the 3D printability of surimi-starch systems. *Food Chemistry*, 374, Article 131727. <https://doi.org/10.1016/j.foodchem.2021.131727>
- Liu, Y., Zhang, Y., Cai, L., Zeng, Q., & Wang, P. (2024). Protein and protein-polysaccharide composites-based 3D printing: The properties, roles and opportunities in future functional foods. *International Journal of Biological Macromolecules*, 272, Article 132884. <https://doi.org/10.1016/j.ijbiomac.2024.132884>
- Loi, C. C., Eyres, G. T., & Birch, E. J. (2019). Effect of mono- and diglycerides on physical properties and stability of a protein-stabilised oil-in-water emulsion. *Journal of Food Engineering*, 240, 56–64. <https://doi.org/10.1016/j.jfoodeng.2018.07.016>
- Lu, C., Ling, Z., Wang, C., Wang, J., Yong, Q., & Chu, F. (2022). Multiple hydrogen bonding interactions toward rapidly self-healing, photothermal conversion elastomer composites. *Composites Part B: Engineering*, 228, Article 109428. <https://doi.org/10.1016/j.compositesb.2021.109428>
- Luo, N., Ye, A., Wolber, F. M., & Singh, H. (2019). Structure of whey protein emulsion gels containing capsaicinoids: Impact on in-mouth breakdown behaviour and sensory perception. *Food Hydrocolloids*, 92, 19–29. <https://doi.org/10.1016/j.foodhyd.2019.01.019>
- Maier, C., Zeeb, B., & Weiss, J. (2014). Investigations into aggregate formation with oppositely charged oil-in-water emulsions at different pH values. *Colloids and Surfaces B: Biointerfaces*, 117, 368–375. <https://doi.org/10.1016/j.colsurfb.2014.03.012>
- McClements, D. J. (2016). *Food emulsions: Principles, practices, and techniques*. CRC Press.
- Morgan, P. T., Witard, O. C., Højfeldt, G., Church, D. D., & Breen, L. (2023). Dietary protein recommendations to support healthy muscle ageing in the 21st century and beyond: Considerations and future directions. *Proceedings of the Nutrition Society*, 1–14. <https://doi.org/10.1017/S0029665123003750>
- Mu, R., Wang, B., Lv, W., Yu, J., & Li, G. (2023). Improvement of extrudability and self-support of emulsion-filled starch gel for 3D printing: Increasing oil content. *Carbohydrate Polymers*, 301, Article 120293. <https://doi.org/10.1016/j.carbpol.2022.120293>
- Olsmats, E., & Rennie, A. R. (2024). Pea protein [*Pisum sativum*] as stabilizer for oil/water emulsions. *Advances in Colloid and Interface Science*, 326, Article 103123. <https://doi.org/10.1016/j.cis.2024.103123>
- Pan, H., Pei, F., Ma, G., Ma, N., Zhong, L., Zhao, L., & Hu, Q. (2022). 3D printing properties of *Flammulina velutipes* polysaccharide-soy protein complex hydrogels. *Journal of Food Engineering*, 334, Article 111170. <https://doi.org/10.1016/j.jfoodeng.2022.111170>
- Reche, C., Umana, M., Dalmau, E., Carcel, J. A., & Eim, V. (2024). Improving 3D printed food characteristics by using mushroom by-products and olive oil in the formulation. *LWT*, 202, Article 116238. <https://doi.org/10.1016/j.lwt.2024.116238>
- Shanthakumar, P., Klepacka, J., Bains, A., Chawla, P., Dhull, S. B., & Najda, A. (2022). The current situation of pea protein and its application in the food industry. *Molecules*, 27(16), 5354. <https://doi.org/10.3390/molecules27165354>
- Sharma, R., Chandra Nath, P., Kumar Hazarika, T., Ojha, A., Kumar Nayak, P., & Sridhar, K. (2024). Recent advances in 3D printing properties of natural food gels: Application of innovative food additives. *Food Chemistry*, 432, Article 137196. <https://doi.org/10.1016/j.foodchem.2023.137196>
- Tarrega, A., Ramírez-Sucre, M. O., Vélez-Ruiz, J. F., & Costell, E. (2012). Effect of whey and pea protein blends on the rheological and sensory properties of protein-based systems flavoured with cocoa. *Journal of Food Engineering*, 109(3), 467–474. <https://doi.org/10.1016/j.jfoodeng.2011.11.003>
- Wang, Y., Liu, Q., Yang, Y., Qiu, C., Jiao, A., & Jin, Z. (2023). Impact of pH on pea protein-hydroxypropyl starch hydrogel based on interpenetrating network and its application in 3D-printing. *Food Research International*, 170, Article 112966. <https://doi.org/10.1016/j.foodres.2023.112966>
- Wang, H., Ouyang, Z., Hu, L., Cheng, Y., Zhu, J., Ma, L., & Zhang, Y. (2022). Self-assembly of gelatin and phycocyanin for stabilizing thixotropic emulsions and its effect on 3D printing. *Food Chemistry*, 397, Article 133725. <https://doi.org/10.1016/j.foodchem.2022.133725>
- Wong, D., Vasanthan, T., & Ozimek, L. (2013). Synergistic enhancement in the co-gelation of salt-soluble pea proteins and whey proteins. *Food Chemistry*, 141(4), 3913–3919. <https://doi.org/10.1016/j.foodchem.2013.05.082>

- Xia, B., Shen, Y., Zhao, R., Deng, J., & Wang, C. (2024). Interactions with soy lecithin regulate the emulsification capacity of pea protein: Effects of soy lecithin concentration. *Food Hydrocolloids*, 155, Article 110168. <https://doi.org/10.1016/j.foodhyd.2024.110168>
- Xu, M., & Dumont, M.-J. (2015). Evaluation of the stability of pea and canola protein-based hydrogels in simulated gastrointestinal fluids. *Journal of Food Engineering*, 165, 52–59. <https://doi.org/10.1016/j.jfoodeng.2015.04.033>
- Ye, T., Chen, X., Li, Q., Chen, Z., Lin, L., Zheng, Z., & Lu, J. (2024). Towards more sustainable surimi gels: Deciphering the hybrid gelation of myofibrillar/plant proteins. *Food Hydrocolloids*, 146, Article 109189. <https://doi.org/10.1016/j.foodhyd.2023.109189>
- Yu, J., Li, D., Wang, L., & Wang, Y. (2023). Improving freeze-thaw stability and 3D printing performance of soy protein isolate emulsion gel inks by guar & xanthan gums. *Food Hydrocolloids*, 136, Article 108293. <https://doi.org/10.1016/j.foodhyd.2022.108293>
- Yu, J., Wang, X., Li, D., Wang, L., & Wang, Y. (2022). Development of soy protein isolate emulsion gels as extrusion-based 3D food printing inks: Effect of polysaccharides incorporation. *Food Hydrocolloids*, 131, Article 107824. <https://doi.org/10.1016/j.foodhyd.2022.107824>
- Zhang, D., Chen, D., Patel, B., & Campanella, O. H. (2022a). Pectin as a natural agent for reinforcement of pea protein gel. *Carbohydrate Polymers*, 298. <https://doi.org/10.1016/j.carbpol.2022.120038>
- Zhang, S., Han, J., Kwok, E., Kan, X., Iordache, M., & Chen, L. (2025). The impact of κ-carrageenan on the pea protein gelation by high pressure processing and the gelling mechanisms study. *Food Hydrocolloids*, 158, Article 110577. <https://doi.org/10.1016/j.foodhyd.2024.110577>
- Zhang, Z., Kobata, K., Pham, H., Kos, D., Tan, Y., Lu, J., & McClements, D. J. (2022b). Production of plant-based seafood: Scallop analogs formed by enzymatic gelation of pea protein-pectin mixtures. *Foods*, 11(6), 851. <https://doi.org/10.3390/foods11060851>
- Zhang, M., Zhang, B., Sun, X., Liu, Y., Yu, Z., Wang, X., & Xu, N. (2024). Freeze-thaw stability of transglutaminase-induced soy protein-maltose emulsion gel: Focusing on morphology, texture properties, and rheological characteristics. *International Journal of Biological Macromolecules*, 261, Article 129716. <https://doi.org/10.1016/j.ijbiomac.2024.129716>
- Zhao, X., Li, D., Wang, L., & Wang, Y. (2022). Rheological properties and microstructure of a novel starch-based emulsion gel produced by one-step emulsion gelation: Effect of oil content. *Carbohydrate Polymers*, 281, Article 119061. <https://doi.org/10.1016/j.carbpol.2021.119061>
- Zhu, P., Chu, Y., Yang, J., & Chen, L. (2024). Thermally reversible emulsion gels and high internal phase emulsions based solely on pea protein for 3D printing. *Food Hydrocolloids*, 157, Article 110391. <https://doi.org/10.1016/j.foodhyd.2024.110391>
- Zhu, P., Huang, W., & Chen, L. (2022). Develop and characterize thermally reversible transparent gels from pea protein isolate and study the gel formation mechanisms. *Food Hydrocolloids*, 125, Article 107373. <https://doi.org/10.1016/j.foodhyd.2021.107373>